JPhys Photonics

Few-cycle high-harmonic generation in liquids: *in-operando* thickness measurement of flat microjets

View the article online for updates and enhancements.

Journal of Physics: Photonics

PAPER

Few-cycle high-harmonic generation in liquids: *in-operando* thickness measurement of flat microjets

Zhong Yin[1] , Tran Trung Luu[1,2] and Hans Jakob Wörner[1]

[1] Laboratorium für Physikalische Chemie, ETH Zürich, 8093, Zürich, Switzerland
[2] Department of Physics, The University of Hong Kong, Pokfulam Road, SAR Hong Kong, People's Republic of China
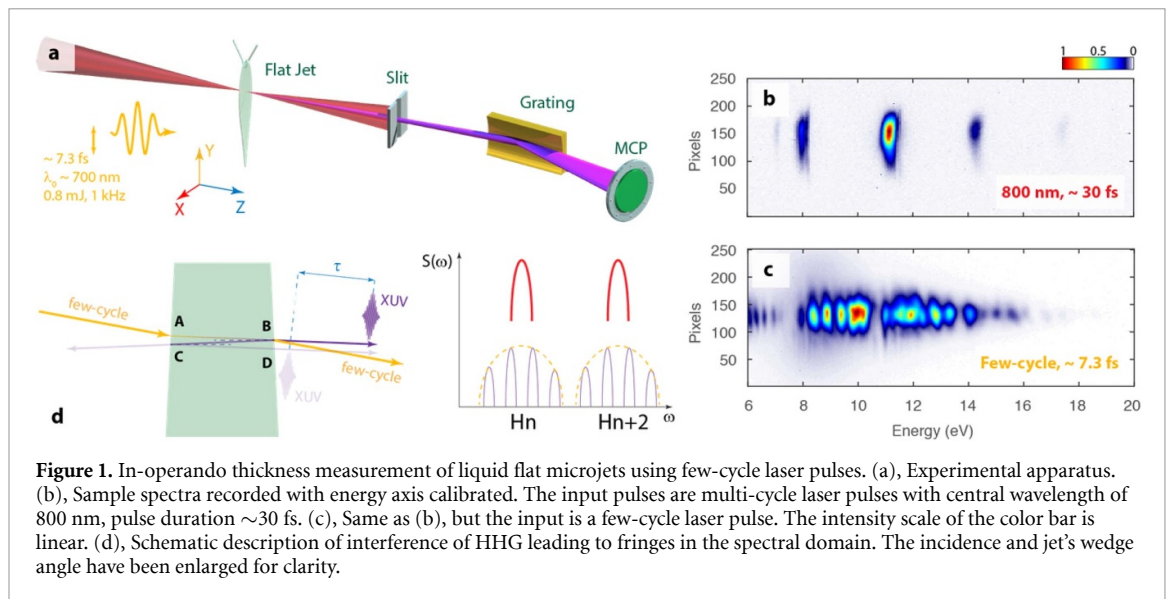
E-mail: ttluu@hku.hk

Abstract

Extreme ultraviolet high-harmonic generation (HHG) from bulk liquids has only recently been demonstrated (T.T. Luu, Z. Yin *et al*, Nat. Comm. 9, 3724, (2018)). This has opened new prospects for the development of bright high-harmonic sources and the development of liquid-phase high-harmonic spectroscopy (HHS). Here, we report on the first observation of HHG in liquids driven by few-cycle (∼7 fs) pulses. We observe the emission of a broad quasi-continuum in the extreme ultraviolet, which is strongly modulated on a photon-energy scale much finer than the central photon energy of the driver. We show that these modulations arise from an etalon effect inside the flat microjet, which we use to perform an in-operando measurement of the flat-jet's thickness. The possibility to directly characterize flat microjets during HHG will greatly support their optimization for light-source applications and facilitate the development of liquid-phase HHS.

1. Introduction

High-harmonic generation (HHG) and high-harmonic spectroscopy (HHS) played an essential role in modern ultrafast science. Studies of electronic properties and dynamics of atoms [1–3], molecules [4–8], and solids [9–13], have substantially benefited from the development of HHG and HHS. In all of these experiments, the high time resolution is a consequence of the interaction of the strong laser field with gases or solids. In order to extend the current techniques of attosecond science to the liquid phase, HHS is a promising avenue. Although there have been efforts to generate high harmonics from water droplets [14], or surface plasma created at extreme intensities [15], HHG from the bulk of liquids was largely limited to the perturbative regime and the visible range [16] of the electromagnetic spectrum until recently. In our recent work [17], we have demonstrated generation of extreme-ultraviolet (XUV) high harmonics from the bulk of water and several alcohols up to 20 eV and its potential application in liquid-phase HHS.

The desire to create free-flowing, well-controlled and ultrathin liquid samples for x-ray spectroscopy has fueled the development of flat microjets, which have reached micro- [18] and nanometer thicknesses [19]. Since the thickness of the sample is of paramount importance to absorption spectroscopy, HHG and HHS, precise characterization techniques are required. In previous work [18], the authors used spectral confocal interferometry. This has the advantage of being a very precise measurement technology. However, it requires the working distance to be on the order of millimeters and is thus impractical for measurements in vacuum, especially under the working conditions of typical experiments. In another work [19], the authors used spectral reflectance and extracted the thickness information by measuring the reflectance spectrum and comparing it with calculations. They additionally used the measured absorbance to determine the thickness. Considering the fact that the flat microjets are made of highly volatile liquids, it is essential to develop characterization approaches that are applicable to high-vacuum conditions. Moreover, the intense laser-liquid interaction required for HHG also potentially modifies the thickness of the jet through enhanced evaporation or laser-induced desorption. In this work, we demonstrate a new thickness measurement technique of liquid flat microjets using HHG driven by few-cycle laser pulses. The key idea of our work is to

Figure 1. In-operando thickness measurement of liquid flat microjets using few-cycle laser pulses. (a), Experimental apparatus. (b), Sample spectra recorded with energy axis calibrated. The input pulses are multi-cycle laser pulses with central wavelength of 800 nm, pulse duration ∼30 fs. (c), Same as (b), but the input is a few-cycle laser pulse. The intensity scale of the color bar is linear. (d), Schematic description of interference of HHG leading to fringes in the spectral domain. The incidence and jet's wedge angle have been enlarged for clarity.

use the broad bandwidth provided by the few-cycle laser pulses to perform white-light interferometry. We discuss different existing numerical methods for the extraction of the thickness, and we identify the most reliable method that combines the strengths of several standard methods. We anticipate our work to be valuable for the further development of the liquid flat microjets. The precise measurement illustrated by our work will help with the determination of physical quantities and processes underlying HHG experiments in liquids.

2. Experiments

The experimental apparatus and key idea of our work are shown in figure 1. In our experiment, the apparatus is aligned such that quick switching between few- and multi-cycle laser pulses is possible. The laser system provides pulses with a central wavelength of 800 nm, a pulse duration of approximately 30 fs and few mJ pulse energy. We used a hollow-core fiber compressor [20] with one meter length, 300 μm core size and 8 reflections on chirped mirrors (PC70—Ultrafast Innovations). Using argon as interaction medium at a pressure of 300 mbar, few-cycle laser pulses are generated with pulse duration of 7.3 fs ± 10%. The pulse durations were precisely measured using a home-made Transient Grating—Frequency Resolved Optical Gating (TG-FROG) device [21]. We note that the exact pulse duration is not required to extract the thickness information. The pulse characterization acts merely as a confirmation of the bandwidth needed for the thickness measurement.

The laser pulses are focused onto a liquid flat microjet placed inside a vacuum chamber. Experiments have been carried out both with the compressed (∼7.3 fs), few-cycle laser pulses, and the multi-cycle (∼30 fs) laser pulses provided by the commercial laser system. The flat microjet is prepared as described in [17], using pure ethanol as the liquid medium and the diameter of the cylindrical jets is ∼27 μm, running at the flow rate of 3.5 ml per minute. An XUV spectrometer consisting of a slit, a flat-field grating and a multi-channel plate (MCP) in combination with a phosphor screen and a charge-coupled device (CCD) camera are used for spectral readout.

Sample spectra obtained with multi-cycle or few-cycle driving laser pulses are shown in figures 1(b) and (c), respectively. Whereas the spectrum obtained with few-cycle driving pulses show strong fringes within the spectral width of each harmonic peak, such fringes are clearly not visible on the harmonics in figure 1(b). The interference mechanism responsible for the observed fringes is illustrated in figure 1(d). It consists in two-fold partial reflection at the liquid-vacuum interfaces, which creates a delayed replica of the generated attosecond pulse train (APT). In other words, the observed fringes are caused by an etalon effect. As we discuss below, the thickness extraction is not trivial because of the broad bandwidth of the few-cycle laser pulses and the spectral/temporal periodicities of the APT.

3. Results and discussions

We first discuss the case of a multi-cycle driving pulse, taking into account the change of refractive index and harmonic bandwidth. In addition, for the sake of visibility, we assume that the angle of incidence is large,

although in practice it is very close to normal incidence. Upon entering the flat microjet at the interface point A, the laser beam will be refracted and will propagate along the AB direction. The refraction angle is determined by the angle of incidence and the refractive index of the flat microjet with respect to the incoming beam. In our experiments, it is very close to zero degrees. For simplicity, since we are only considering transmitted beams which reach the XUV spectrometer, we neglect all of the reflected beams including possible HHG signals generated at the surface [22, 23]. During propagation of the laser beam from A to B, strong-field laser-liquid interaction will give rise to HHG accumulating during propagation, as depicted by the gradient color code. At the interface point B, a fraction of the laser beam will be refracted out, in a direction parallel to the incoming beam since the surfaces on the flat microjet only have a very small wedge angle. However, the harmonics will be refracted out at a slightly different angle due to different refractive indices at the visible/infrared and XUV wavelengths [24]. As one would expect from thin-film optics, a fraction of the harmonics is not transmitted completely, but reflected internally. This radiation propagates along the B-C-D path and eventually leaves the jet in a direction (almost) parallel to the first emitted APT. This replica of the APT interferes with the first APT, thereby generating the fringes observed in the XUV spectrum. Due to the strong intensity reduction, short duration of the laser pulses, and phase matching, the non-linear optical effects between the near-infrared and the first reflected XUV are expected to be weak, therefore they are not being considered further in this work. It is important to note that the width of the harmonics (for example, Hn and Hn + 2) strongly depends on the bandwidth of the incoming laser pulse. If the incoming beam is multi-cycle (red colour) then the harmonics will be narrow, but they will be much broader when generated from the few-cycle pulse (dark yellow colour). In addition, the spacing between the interference fringes depends only on the time delay between the first APT and its delayed replica. If this spacing is much smaller than the HHG bandwidth, interference fringes will not be seen. The practical limit of thickness detectable by this method is defined by the maximum bandwidth of the broad harmonics and the resolution of the spectrometer. In this case, these are approximately 1.5 eV and 0.2 eV, repsectively, which corresponds to a thickness range from approximately 275 nm to 2.1 μm. In fact, a rough estimation of the propagation time using the refractive index and optical path length shows that a delay of 20 fs would correspond to the liquid flat microjet thickness of more than 2 μm. Since our flat microjets are much thinner, as shown below, fringes are not observed in HHG driven by the multi-cycle laser pulses. In contrast, when the incoming beam is a few-cycle laser pulse, the harmonic bandwidth is broad enough to support the interference pattern. As a result, interference fringes can be measured as shown in figure 1(c). Since any further reflection inside the jet would further reduce the intensity of the reflected/transmitted beam, it is safe to assume that the total interference signal is made from only the first and the second, without significant amounts of higher-order reflections of the APT. Hence the time delay causing the interference signal is purely linked to the propagation time of the APT inside the flat microjet over two times its thickness.

It is important to make sure that it is the APT reflecting twice and propagating inside the jet that causes the observable interference, not the laser pulse. Since the fundamental laser pulse also reflects twice and propagates inside the jet, it might generate significant APT afterward to interfere with the first APT transmitted. We have performed detailed intensity reduction calculations on these two possible mechanisms and the results are in agreement with the attenuation length extracted from measured oscillator strengths to within one order of magnitude. An XUV pulse centered at 9 eV will have its intensity reduced by ~17.8 times after propagation over 1.6 μm. Here, and it what follows, we use the complex refractive index of water at 9 eV because that of ethanol has not been reported. Taking into account the loss due to Fresnel's formula after two internal reflections with an attenuation of ~614.8 times each, the total loss is ~10 974 times. Similarly, using the refractive index of ethanol at 700 nm (central carrier wavelength of the few-cycle pulse) with a real part of 1.329 and an imaginary part of 1 (negligible absorption of the carrier wave propagating inside the jet), the loss due to double internal reflection amounts to a factor of 2511. In addition, we assume that the effective nonlinearity of generating H5 is approximately ofthird order, extrapolating from the results obtained in [17]. This leads to the total reduction of the APT generated by the doubly reflected driving field by the third power of 2511 or ~1.58 × 1010 times. To conclude, comparing this loss with the loss of about 104 calculated above, it is evident that the observed interference is generated mainly between the double internal reflection of the APT and the directly transmitted APT.

In principle, one can also use the fringe visibility to learn about the intensity ratio between the two involved electric fields. In our experimental data, the visibility ranges from approximately 16% to 36% which corresponds to an intensity ratio of ~30 to 150, which is off by more than one order of magnitude compared to the estimated value due to absorption coefficient of water. At least three points can be considered to explain this: (i) the intensity reduction due to absorption is exponentially dependent on the absorbance, such that a tiny difference in the absorption coefficient can cause a large change in the transmitted intensity; (ii) the refractive-index data we used is for water, because of a lack of relevant data for ethanol; (iii) Partial
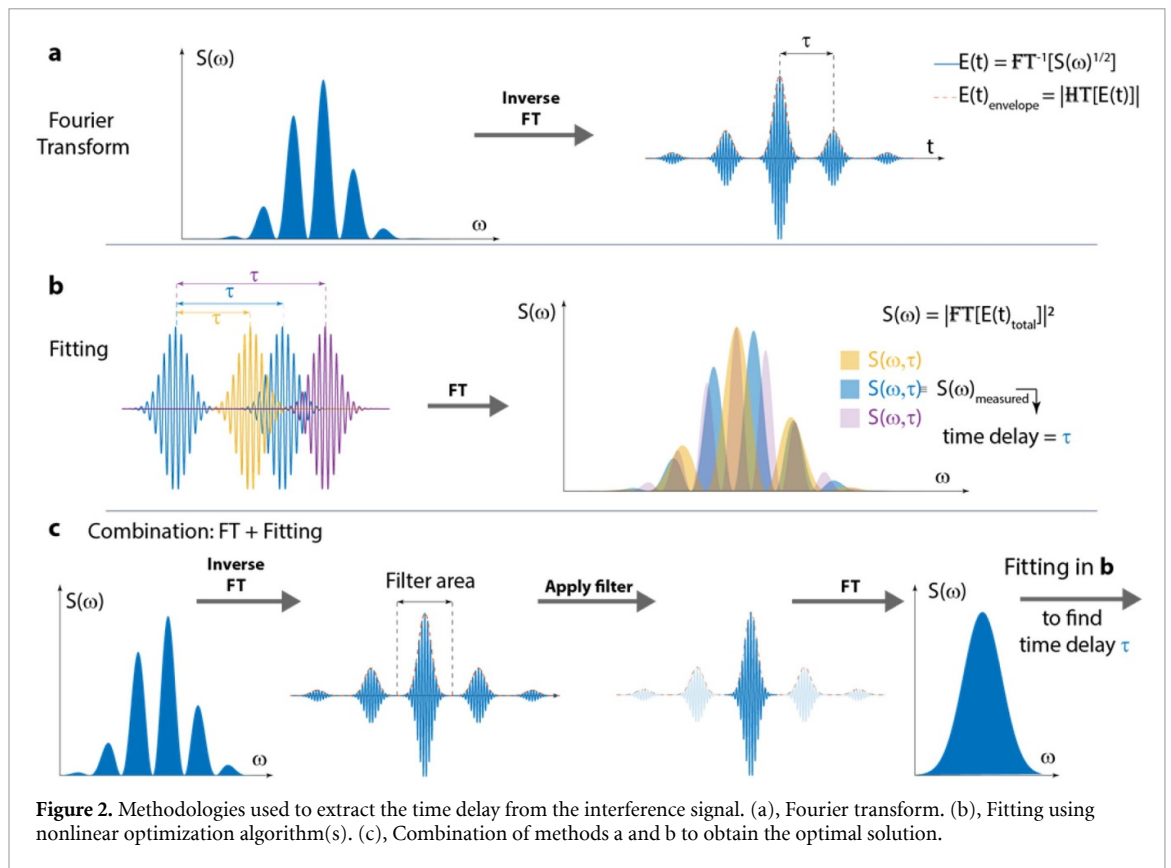
Figure 2. Methodologies used to extract the time delay from the interference signal. (a), Fourier transform. (b), Fitting using nonlinear optimization algorithm(s). (c), Combination of methods a and b to obtain the optimal solution.

coherence between the two APTs will also reduce the fringe contrast. As a consequence, the fringe visibility might not be the best tool to infer the refractive index or thickness of the liquid in this case.

4. Thickness extraction

From the above considerations, the thickness L of the flat microjet can be directly linked to the time delay between the APTs as $L = \frac{c\tau}{2n}$ where c is the speed of light, n is the refractive index of the jet for the relevant XUV wavelength. Since the APT is reflected at point C from a higher refractive index (liquid jet) to the lower refractive index (vacuum), there is also no additional phase shift.

Three methods that can be used to extract the time delay τ from the interference fringes are illustrated in figure 2. In the first method, which we call pure Fourier transform in figure 2(a), the interference spectrum $S(\omega)$ is initially inverse-Fourier-transformed to obtain the time domain representation $E(t) = FT^{-1}[S(\omega)^{1/2}]$. Then the envelope function of the electric field can be obtained using the Hilbert transform $E(t)_{envelope} = |HT[E(t)]|$. The time delay can be extracted as a simple temporal separation between the central and the first peak on either side of the envelope function. Mathematically this should be the most accurate way to obtain the time delay between the two pulses from the interference spectrum. Practically, the precision of this method depends strongly on the shape of $S(\omega)$ when performing the inverse Fourier transform. For interferometry with a true white-light spectrum the method does not depend on the bandwidth of $S(\omega)$. However, in our case, the high-harmonic spectrum serves as 'white light', which leads to some challenges: (i) if the bandwidth of $S(\omega)$ used in the (inverse) Fourier transform is larger than the separation of the harmonics, the temporal periodicity of the APT will be reflected in the Fourier transformed signal E(t). (ii) The shape of the harmonics influences the shape of the temporal envelope function such that it is not a Gaussian or any easy-to-find-peak function. Finding the absolute time delay between the peaks of the temporal envelope function is no longer trivial. (iii) The contrast of the measured spectral fringes and the overall quality of the measurements: finding the local maxima on the temporal envelope function depends highly on the fringe contrast and other experimental parameters. (iv) The precision of the method depends on the sampling of the frequency-domain representation. For instance, if the maximally considered energy is 10 eV in our spectra, this corresponds to the temporal grid step of ~207 attoseconds or 21 nanometers as the precision for the thickness we would retrieve. For our case, even though (iv) is small and we intentionally limit S(ω) to properly cover only one harmonic to minimize the limitations from (i), other challenges from (ii) and (iii) are very serious and they render the first method inaccurate for our purpose.
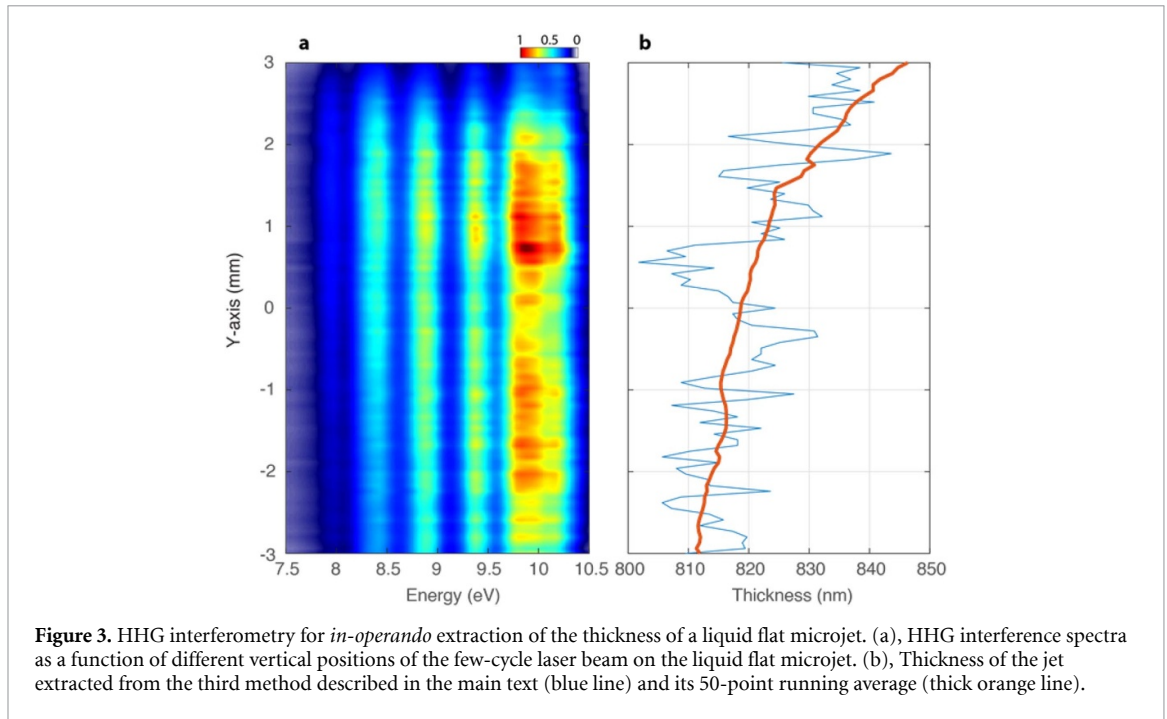
Figure 3. HHG interferometry for *in-operando* extraction of the thickness of a liquid flat microjet. (a), HHG interference spectra as a function of different vertical positions of the few-cycle laser beam on the liquid flat microjet. (b), Thickness of the jet extracted from the third method described in the main text (blue line) and its 50-point running average (thick orange line).

The second method that is also widely used is nonlinear optimization or fitting. In this approach, as depicted in figure 2(b), we first simulate a pair of XUV pulses, separated by a variable time delay τ. The corresponding spectrum is then calculated as $S(\omega) = |FT[E(t)_{total}]|^2$. By scanning the time delay τ until the best match with the experimentally measured interference spectrum is found, τ can be determined. Although this method does not suffer from the above problems (i) and (iv), it still suffers from (ii) and (iii) and a newly raised problem (v): since we do not know the actual temporal profile of the harmonics, simulating them assuming any given shape will add a new source of error to the fitting.

Considering the above limitations of the described methods, we combine the advantages of each of these methodologies into a mixed approach. In this approach, illustrated in figure 2(c), the interference spectrum is first inverse-Fourier-transformed as in figure 2(a). However, instead of taking immediately the envelope function and extracting the temporal separation, we isolate only the area under the main, central peak and perform the ordinary Fourier transform to get back a spectrum. Together with selecting the bandwidth for S(ω) properly in the beginning, this approach allows us to extract precisely the shape of the harmonic under investigation. In this way, we circumvent problem (i), (ii), and partially problem (v): we have the spectrum but not the spectral phase so we have only half of the information needed to solve (v). In the next step, we use this filtered spectrum as a base to do the fitting of the interference spectra. By using fitting, we immediately eliminate problem (iv). In order to minimize the last problem, (iii), we introduce a few additional fitting parameters: $E(t)_{total} = E(t) + P_1 \times E(t - P_2)^* \exp(iP_3)$ where P_1 is the amplitude scaling factor, P_2 is the time delay, P_3 is the phase offset due to propagation inside the jet. The thickness extracted as the result of fitting is shown in figure 3 below.

We note that in order to minimize problem (i), the spectral bandwidth used for the Fourier transform in the first step is truncated to the first five fringes as illustrated in figure 3(a). Here, the raw interference signal does not change much as a function of the vertical position. This suggests that there is little change of the thickness. Indeed, the extracted results, shown in figure 3(b), corroborate this suggestion. The determined thickness of the flat microjet is almost constant, showing evidence of a slight decrease from ∼840 nm at the top to ∼810 nm at the bottom. As stated above, to the best of our knowledge, refractive index measurements of ethanol in this spectral range are currently not available. Therefore, the refractive index of water has been used for the calculation of the thickness instead. Assuming that the refractive index of ethanol at 9 eV will be measured (as R) in the future, the real thickness can be obtained by dividing the thickness reported here by R/1.503, where 1.503 is the refractive index of water (real part) at 9 eV. By performing multiple fitting using different initial guesses, the results are converged to a precision of ∼20 nm or less. This is remarkable as it exceeds the resolution allowed by standard Fourier transform (the first method) which amounts to ∼60 nm and it additionally supports our choice to use fitting to overcome the problem of the limited sampling in the spectral domain (iv). In addition, the results of the fit can not only provide the thickness information of the

jet, but also information on the propagation of the HHG as well as characteristics of the HHG emitted from liquids. This is beyond the scope of this work and will be discussed in a follow-up paper.

The precision of the extraction can also be estimated directly. Since our XUV pulses are short APTs, the change of the carrier-envelope phase (CEP) of the driver is virtually identical to a shift of the XUV temporal profile in time. As a result, both a change of driving-field CEP and a change of the temporal delay (reflecting the thickness of the flat microjet) would cause an energetic shift of the spectral fringes. The fringes would shift by one complete fringe spacing as the CEP is changed by 2π or the temporal delay changes by one period of the carrier wave. In this case, the carrier wave is the 5th harmonic of the few-cycle driver, its energy is approximately 9 eV and thus the corresponding carrier wavelength is $\sim$140 nm. In figure 3(a), no large shift of the spectral fringes is observed. All fringes are largely unchanged upon scanning the flat microjet vertically over several millimeters. Therefore, by comparing the actual energy shift to the distance between the fringes, one can safely conclude that the change of the thickness is very small in comparison to one wavelength. The precision of the extraction, hence, is on the order of 20 nm or even better. This agrees with the results obtained by numerical treatment presented in the previous paragraph. In addition, the uncertainty due to the dependence of the fitted frequency on the signal-to-noise ratio is rather small, on the order of 1%, thus it can be safely neglected.

5. Conclusions

We have demonstrated a methodology to perform a thickness measurement during HHG in liquid flat microjets. By exploiting the large bandwidth of few-cycle laser pulses, interference fringes have been observed in the emitted HHG spectra, which can be directly linked to the thickness of the flat microjet. We described three possible methods for the thickness determination and showed that the most reliable technique is the combination of Fourier transform and nonlinear optimization. The extracted thickness of the flat microjet lies in the range of 810–840 nm when created with cylindrical jets of $\sim$27 μm diameter and a flow rate of 3.5 ml per minute. With a precision of $\sim$20 nm or better, our methodology is a promising, precise way to characterize the thickness of flat microjets. In addition, precise measurements of this type open the door for comprehensive studies of propagation effects inside the liquid jet. As a result, it could play an important role in further optimization of flat-microjet-based high-harmonic sources and studies of electronic structure and dynamics of liquids using HHS.

Disclosures

The authors declare no conflicts of interest.

ORCID iDs

Zhong Yin ● https://orcid.org/0000-0001-5594-9879
Tran Trung Luu ● https://orcid.org/0000-0003-3772-3379
Hans Jakob Wörner ● https://orcid.org/0000-0002-8877-0872

References

[1] Hentschel M, Kienberger R, Spielmann C, Reider G A, Milosevic N, Brabec T, Corkum P, Heinzmann U, Drescher M and Krausz F 2001 Attosecond metrology *Nature* **414** 509–13
[2] Drescher M, Hentschel M, Kienberger R, Uiberacker M, Yakovlev V, Scrinzi A, Westerwalbesloh T, Kleineberg U, Heinzmann U and Krausz F 2002 Time-resolved atomic inner-shell spectroscopy *Nature* **419** 803–7
[3] Schultze M *et al* 2010 Delay in photoemission *Science* **328** 1658–62

[4] Itatani J, Levesque J, Zeidler D, Niikura H, Pépin H, Kieffer J C, Corkum P B and Villeneuve D M 2004 Tomographic imaging of molecular orbitals *Nature* **432** 867–71

[5] Huppert M, Jordan I, Baykusheva D, von Conta A and Wörner H J 2016 Attosecond delays in molecular photoionization *Phys. Rev. Lett.* **117** 093001

[6] Niikura H, Légaré F, Hasbani R, Bandrauk A D, Ivanov M Y, Villeneuve D M and Corkum P B 2002 Sub-laser-cycle electron pulses for probing molecular dynamics *Nature* **417** 917–22

[7] Kraus P M *et al* 2015 Measurement and laser control of attosecond charge migration in ionized iodoacetylene *Science* **350** 790–5

[8] Worner H J, Bertrand J B, Kartashov D V, Corkum P B and Villeneuve D M 2010 Following a chemical reaction using high-harmonic interferometry *Nature* **466** 604–7

[9] Ghimire S, DiChiara A D, Sistrunk E, Agostini P, DiMauro L F and Reis D A 2010 Observation of high-order harmonic generation in a bulk crystal *Nat. Phys.* **7** 138–41

[10] Schubert O *et al* 2014 Sub-cycle control of terahertz high-harmonic generation by dynamical Bloch oscillations *Nat. Photon.* **8** 119–23

[11] Luu T T, Garg M, Kruchinin S Y, Moulet A, Hassan M T and Goulielmakis E 2015 Extreme ultraviolet high-harmonic spectroscopy of solids *Nature* **521** 498–502

[12] Yoshikawa N, Tamaya T and Tanaka K 2017 High-harmonic generation in graphene enhanced by elliptically polarized light excitation *Science* **356** 736–8

[13] Hafez H A *et al* 2018 Extremely efficient terahertz high-harmonic generation in graphene by hot Dirac fermions *Nature* **561** 507–11

[14] Flettner A, Pfeifer T, Walter D, Winterfeldt C, Spielmann C and Gerber G 2003 High-harmonic generation and plasma radiation from water microdroplets *Appl. Phys.* B **77** 747–51

[15] Heissler P *et al* 2014 Using the third state of matter: high harmonic generation from liquid targets *New J. Phys.* **16** 113045, 1-10

[16] DiChiara A D, Sistrunk E, Miller T A, Agostini P and DiMauro L F 2009 An investigation of harmonic generation in liquid media with a mid-infrared laser *Opt. Express* **17** 20959–65

[17] Luu T T, Yin Z, Jain A, Gaumnitz T, Pertot Y, Ma J and Wörner H J 2018 Extreme-ultraviolet high-harmonic generation in liquids *Nat. Commun.* **9** 3723

[18] Ekimova M, Quevedo W, Faubel M, Wernet P and Nibbering E T J 2015 A liquid flatjet system for solution phase soft-x-ray spectroscopy *Struct. Dyn.* **2** 054301

[19] Koralek J D *et al* 2018 Generation and characterization of ultrathin free-flowing liquid sheets *Nat. Commun.* **9** 1353

[20] Nisoli M, De Silvestri S and Svelto O 1996 Generation of high energy 10 fs pulses by a new pulse compression technique *Appl. Phys. Lett.* **68** 2793–5

[21] Sweetser J N, Fittinghoff D N and Trebino R 1997 Transient-grating frequency-resolved optical gating *Opt. Lett.* **22** 519–21

[22] Vampa G, Liu H, Heinz T F and Reis D A 2019 Disentangling interface and bulk contributions to high-harmonic emission from solids *Optica* **6** 553-556

[23] Vampa G, You Y S, Liu H, Ghimire S and Reis D A 2018 Observation of backward high-harmonic emission from solids *Opt. Express* **26** 12210-12218

[24] Hayashi H and Hiraoka N 2015 Accurate measurements of dielectric and optical functions of liquid water and liquid benzene in the VUV region (1-100 eV) using small-angle inelastic x-ray scattering *J. Phys. Chem.* B **119** 5609–5623